RESIDUAL OIL SATURATION UNDER MIXED-WET CONDITIONS: OPTIMAL WETTABILITY REVISITED

Magali Christensen, Yukie Tanino
School of Engineering, University of Aberdeen, UK

This paper was prepared for presentation at the International Symposium of the Society of Core Analysts held in Trondheim, Norway, 27-30 August 2018

ABSTRACT

We present laboratory measurements of imbibition capillary pressure and residual oil saturation established by centrifuge in mixed-wet Indiana limestone cores. The capillary pressure curves were combined with previously reported waterflood data [1 - 3] to extract relative permeability curves by history matching. Both centrifuge and waterflood data suggest that residual oil saturation decreases monotonically as contact angle increases from θ_a = 110° to 150°, in contrast to the non-monotonic dependence displayed by core-averaged oil saturation at the end of waterfloods. The results indicate that capillary end effects may be significant even in rock of relatively low permeability, and highlight the importance of using simulation to interpret coreflood data under capillary-dominated conditions.

INTRODUCTION

Salient features of waterflood oil recovery under mixed-wet conditions where the oil-contacted grain surfaces are strongly oil-wet are well established. However, there is no consensus on the optimal wettability for waterflood oil recovery. While some laboratory studies and pore network simulators report the dependence of oil recovery on contact angle, their findings are contradictory, with minimum core-averaged remaining oil saturation after a fixed pore volumes (ranging from 2.4 to 50 pore volumes) of water injected reported near neutral wettability in some studies [4 - 7] and under strongly oil-wet conditions in others [8]. Core-averaged oil saturation established by centrifuge has also been observed to display a minimum at near-neutral wettability [9 as cited in 10, 11].

We present laboratory measurements of imbibition capillary pressure and residual oil saturation established by centrifuge in mixed-wet Indiana limestone cores. Wettability was systematically varied by adding different organic acids to the oil phase. The capillary pressure curves were then combined with previously reported waterflood data [1 - 3] to extract relative permeability curves by history matching.

MATERIALS

Rock

Experiments were performed on 1.5 in.-diameter, 2 in.-long Indiana limestone cores, with a porosity of ϕ = 0.15 and an absolute permeability of k = 5.7 ± 2.0 mD (Table 1). The same batch of cores was used in previous studies [2, 3].

Fluids

An aqueous solution of 5 wt.% NaCl and 1 wt.% KCl, with dynamic viscosity μ_w = 1.109 [12], was used as connate and flood water in all experiments. Three oils were considered: 6.6×10^{-2} M solutions of cyclohexanecarboxylic acid, cyclohexanepropionic acid, and cyclohexanepentanoic acid in *n*-decane. These organic acids alter the wettability of calcite in order of increasing alkyl chain length, resulting in dynamic advancing contact angles of θ_a = 110º, 125º, and 150º [2]. The corresponding interfacial tensions with the brine are σ = 33.10, 28.50, and 16.50 mN/m, respectively [2]. The density of the test fluids was measured at 21°C (Anton Paar 4100M) at the end of primary drainage (Table 1).

METHODS

Initial oil saturation, S_{oi}, was established using the porous plate method, then forced secondary imbibition (increasing water saturation, S_w) capillary pressure curve was measured using the centrifuge method.

Establishment of initial oil saturation

Details of the coreflood apparatus and procedure can be found in Refs. [2, 13, 14]. The key steps were as follows [2]:

1. Each core was alternately evacuated and flushed with gaseous CO_2 to remove air, then flushed with degassed brine to fully saturate it. k was measured.
2. The test oil was injected into the core at constant pressure to establish S_{oi} using the porous plate method.
3. The core was removed from the Hassler cell and weighed to determine S_{oi} by mass balance.

Table 1. Summary of experimental conditions. Density and viscosity are reported for 21°C.

		cores		
		C2	**C1**	**C3**
ϕ		0.155	0.148	0.145
k	mD	6.89 ± 0.11	6.73 ± 0.17	3.44 ± 0.08
θ_a **[2]**	°	110°	125°	150°
σ **[2]**	mN/m	33.10	28.50	16.50
brine density	kg/m^3	1044.6	1045.8	1043.3
oil density	kg/m^3	731.0	732.8	733.0
oil viscosity	mPa s	0.894 [12]	0.877	0.911 [12]
S_{oi}		0.919	0.852	0.886

Forced imbibition capillary pressure measurement by centrifuge

Cores were sent to a commercial laboratory for forced imbibition capillary pressure-saturation measurement by centrifuge (Optima L-100 XP Ultracentrifuge, COREX (UK) Ltd, Aberdeen). Here, the cores were spun at a constant rotational speed of ω = 1060 rpm inside a brine-filled sample holder, and the volume of produced oil measured at selected times using a calibrated glass collector. Once production ceased, viz. equilibrium was established, the rotation speed was increased in discrete steps to ω = 1410, 1850, 3280, 3370, 4460, 5300, and finally 5830 rpm. These speeds correspond to Bond numbers,

$$\mathrm{Bo} = \frac{k\,\omega^2\left(\rho_\mathrm{w} - \rho_\mathrm{o}\right)\left(r_1 + L/2\right)}{\sigma\,\left|\cos\theta_\mathrm{a}\right|}\,, \tag{1}$$

where $r = r_1$ (= 166.3 mm) corresponds to the end of the core closest from the axis of rotation, between Bo = 1.7×10^{-7} and 1.5×10^{-5}. Previous analysis by Masalmeh [15] suggest that Bo is independent of rate over these values, supporting our implicit assumption in our analysis that desaturation of S_or, viz. remobilization of oil trapped at smaller ω, did not take place under the conditions considered presently.

The equilibrium core-averaged saturation, $\langle S_\mathrm{w}\rangle$, is readily determined from the cumulative volume of oil produced at each ω. In addition, for $\theta_\mathrm{a} = 150°$ only, $\langle S_\mathrm{w}\rangle$ at $P_\mathrm{c} = 0$ was predicted from [14]:

$$\langle S_\mathrm{o}\rangle(P_\mathrm{c}{=}0) = (0.9619 \pm 0.06)S_\mathrm{oi} - (0.0729 \pm 0.05) \tag{2}$$

Assuming $P_\mathrm{c} = 0$ at $r = r_1$, the equilibrium capillary pressure distribution within the sample at a particular ω is given by:

$$P_\mathrm{c}(r) = P_\mathrm{o}(r) - P_\mathrm{w}(r) = -\frac{1}{2}\left(\rho_\mathrm{w} - \rho_\mathrm{o}\right)\omega^2\left(r^2 - r_1^2\right). \tag{3}$$

Core analysis software CYDAR™ (CYDAREX) was used to extract the $S_\mathrm{w}(P_\mathrm{c})$ curve such that the corresponding $\langle S_\mathrm{w}\rangle(P_\mathrm{c}(r_1{+}L, \omega))$ best fits measured values using Forbes [16]'s solution of the second kind [16]. Finally, a modified hyperbolic function of the form

$$S_\mathrm{w} = \frac{\beta_3}{\left|P_\mathrm{c}{-}\beta_1\right|^{\beta_4}} + \beta_2\,, \tag{4}$$

where β_1, β_2, β_3, and β_4 are fitting parameters, was fitted to the best-fit $S_\mathrm{w}(P_\mathrm{c})$ in the least squares sense. Residual saturation is taken to be $S_\mathrm{or} = 1 - \beta_2$.

Waterflood relative permeability

Relative permeabilities to oil, k_ro and brine k_rw during selected waterfloods performed in previous studies [1 - 3] were determined by iterative history matching of simulated $\Delta P_\mathrm{w}(t)$ and oil production to measured values using software CYDAR™. P_c^C was scaled using the Leverett-*J* function, i.e.,

$$P_\mathrm{c}\left(\hat{S}_\mathrm{w}\right) = P_\mathrm{c}^\mathrm{C}\left(\hat{S}_\mathrm{w}\right)\sqrt{\frac{k^\mathrm{C}/\phi^\mathrm{C}}{k\,/\phi}}\,, \tag{5}$$

where superscript C denotes properties of cores C1, C2, and C3 on which the $P_\mathrm{c}(S_\mathrm{w})$ were measured and the rescaled water saturation is

$$\hat{S}_\mathrm{w}(t) = \frac{S_\mathrm{w}(t) - S_\mathrm{wi}}{1 - S_\mathrm{wi} - S_\mathrm{or}}\,. \tag{6}$$

Relative permeability was modelled using LET correlations [17]:

$$k_{rw} = k_{rw}(S_{or}) \frac{\hat{S}_w^{\,L_w}}{\hat{S}_w^{\,L_w} + E_w \left(1-\hat{S}_w\right)^{T_w}}, \qquad k_{ro} = k_{ro}(S_{wi}) \frac{\left(1-\hat{S}_w\right)^{L_o}}{\left(1-\hat{S}_w\right)^{L_o} + E_o\, \hat{S}_w^{\,T_o}}, \tag{7}$$

where S_{or}, S_{wi}, $k_{rw}(S_{or})$, $k_{ro}(S_{wi})$, L_i, E_i, and T_i were fitting parameters and i = (o, w).

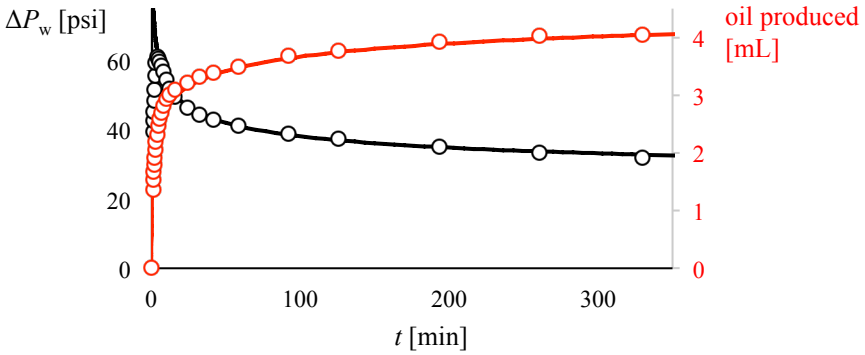

Figure 1. Measured (markers) and simulated (solid line) pressure drop across the length of the core (black) and cumulative oil production (red). U_w = 30 μm/s; θ_w = 150°.

RESULTS

Capillary desaturation curve

Figure 2 presents the core-averaged oil saturation, $\langle S_o \rangle$, at the end of each rotation speed normalized by its value at P_c = 0 as a function of the Bo (solid markers). Superposed are core-averaged remaining oil saturation established by waterflooding from high S_{oi} at constant Darcy velocity, U_w, using the same brine and test oils as those used in the centrifuge experiments. These data are plotted against microscopic capillary number, defined in this paper as:

$$\mathrm{Ca} = \frac{\mu_w\, U_w}{\sigma\, |\cos\theta_a|}. \tag{8}$$

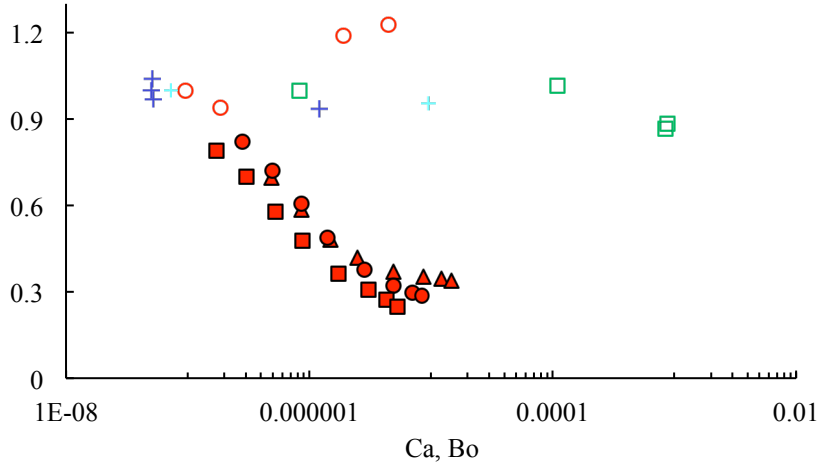

Figure 2 Core-averaged oil saturation normalized by the initial oil saturation, $\langle S_o \rangle / S_{oi}$, at the end of each rotation speed as a function of Bo (solid markers). Superposed are end-point core-averaged oil saturations at the end of waterflood as a function of Ca in Indiana limestone (+, ○) and Ketton limestone (+, □). The ordinate is normalized

by $\langle S_o \rangle / S_{oi}$ at the lowest Ca or Bo considered for that rock in a particular study. Present (centrifuge) experiments: ▲ (θ_a = 110°), ● (125°), and ■ (150°). Waterfloods in Indiana limestone: 6.6×10^{-2} M cyclohexanepropionic acid (○, after 76 – 99 pv of injection; [2]); *n*-decane (+; after 8 – 105 pv of injection [2, 3]). Waterfloods in Ketton limestone: *n*-decane (+; after 19, 343 pv of water injection [13]); 6.6×10^{-2} M cyclohexanepentanoic acid (□; after 105 – 122 pv of water injection [18]).

Measurements in Indiana limestone considered presently and Ketton limestone are included. In Ketton limestone, the critical Ca for desaturation appears to be delayed to at least Ca ~ 10^{-4} (□) at θ_a = 150°. Waterflood remaining oil saturation in Indiana limestone does not display any Ca dependence up to Ca = 1.3×10^{-6} under water-wet conditions (+). Previous studies suggest that the critical Ca for desaturation may be at least one order of magnitude larger under mixed-wet conditions than under water-wet conditions [19], further corroborating our assumption that the centrifuge experiments were not subject to S_{or} remobilization.

Curiously, under mixed-wet conditions, $\langle S_{or} \rangle / S_{oi}$ established by waterflood in Indiana limestone increases with Ca above Ca = 1.8×10^{-7} (○). One possible explanation for this counter-intuitive trend is preferential flow. At higher flow rates, the impact of core-scale heterogeneities may be more pronounced, and the injected brine may preferentially flow through the network of larger pores, bypassing the smaller pores which provide more resistance thus leaving behind a relatively large volume of oil. This is a topic of future study with in-situ visualization at the mm-scale.

Imbibition capillary pressure

Figure 3 presents best-fit imbibition capillary pressure-saturation curves at θ_a = 110°, 125°, and 150° (solid lines). $S_w(P_c)$ displays the canonical profile for imbibition capillary pressure: S_w increases monotonically with increasingly $|P_c|$ at a rate that decreases as $|P_c|$ increases as it approaches its asymptotic limit, viz. residual state.

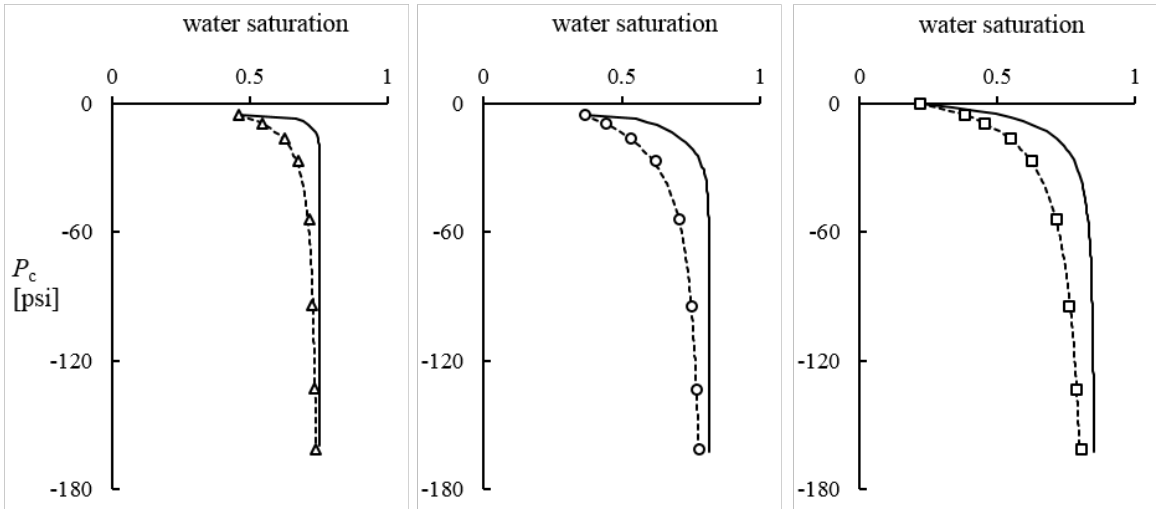

Figure 3. Local ("true") $P_c(S_w)$ (solid line) derived using Forbes [16]'s solution of the second kind such that the corresponding $\langle S_w \rangle(P_c(r_1+L))$ (dashed line) best fits measured $\langle S_w \rangle(P_c(r_1+L))$ at θ_a = 110° (Δ), 125° (○), and 150° (□). Note that the marker at P_c = 0 for θ_a = 150° is predicted from Eq. (2).

Waterflood relative permeability

Figure 4 presents best-fit LET functions for k_{rw} and k_{ro} at U_w = 1.5 (dotted), 3.0 (dashed), and 30 μm/s (solid lines). At constant Ca, $k_{ro}(S_{wi})$ decreases slightly with increasing θ_a, consistent with previous observations (e.g., [3, 8]), suggesting that wettability alteration that takes place during primary drainage affects the pore-scale fluid distribution at S_{oi}. Surprisingly, the optimized $k_{rw}(S_{or})$ does not display a monotonic increase with θ_a. At θ_a = 150° for which the largest and the smallest U_w were considered, $k_{ro}(S_{wi})$ and $k_{rw}(S_{or})$ are a factor of two and seven larger at Ca = 3.4×10^{-6} than at Ca = 1.1×10^{-7}.

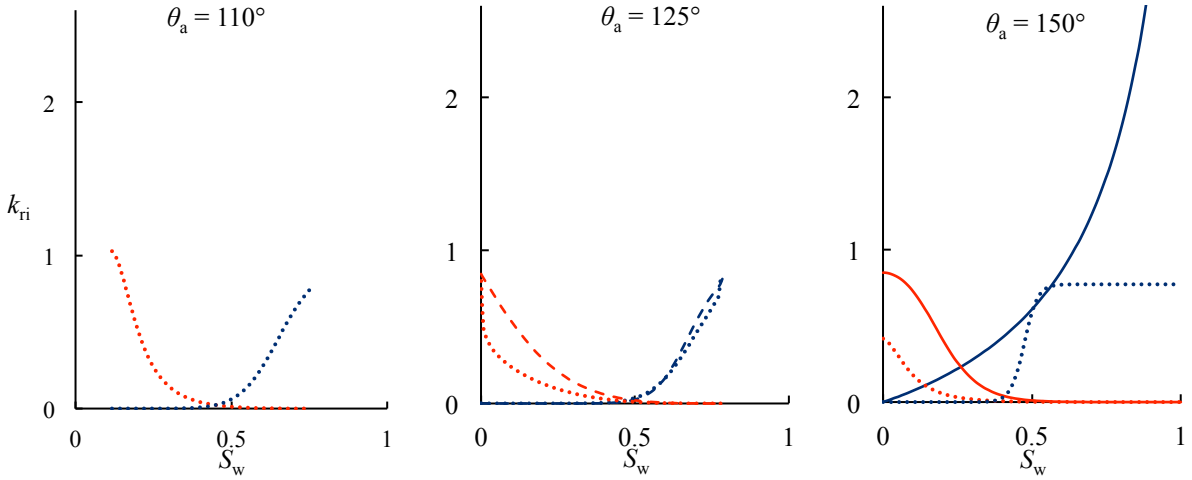

Figure 4. Best-fit LET functions for oil (red) and brine (blue) relative permeabilities [Eq. (7)] at U_w = 1.5 (dotted), 3.0 (dashed), and 30 μm/s (solid lines). Note that only one or two U_w were considered at each θ_a. See Table 2 for values of the best-fit parameters.

Table 2. Summary of relative permeability measurements. Corefloods are a subset of those reported in Refs. [1 - 3]. $\langle S_{or} \rangle$ denotes core-averaged remaining oil saturation at the end of waterflood measured after t pore volumes of water injected.

								best-fit parameters			
Θ_a [°]	**core**	ϕ	L [mm]	k [mD]	S_{oi}	$\langle S_{or} \rangle$ (t [pv])	U_w [μm/s]	$k_{ro}(S_{wi})$	$k_{rw}(S_{or})$	L_w, E_w, T_w	L_o, E_o, T_o
110	W [2]	0.15	88.97	6.3	0.88	0.32 (91)	1.5	1.0 (0.12)	0.79 (0.23)	6.2, 1.1, 0.84	2.4, 22, 1.7
125	O [2]	0.14	88.50	3.8	0.89	0.27 (99)	1.5	0.80 (0)	0.85 (0.22)	9.0, 0.52, 0.22	3.3, 3.2, 0.36
	V [2]	0.15	88.95	8.5	0.87	0.25 (93)	3.0	0.84 (0)	0.82 (0.22)	10.4, 0.48, 0.50	3.0, 3.1, 1.0
150	N [3]	0.15	89.12	11.1	0.82	0.32 (132)	1.5	0.42 (0)	0.77 (0)	8.6, 12.5, 13.9	4.5, 28.0, 1.5
	L13 [1]	0.15	50.98	9.11	0.77	0.29 (116)	45	0.85 (0)	5.5 (0)	1.0, 7.7, 0.97	5.9, 4.4, 1.7

Residual saturation

S_{or} extrapolated from the centrifuge experiments (Fig. 5, Δ) and derived by history matching to waterflood data (red ●) both decrease monotonically with increasing θ_a. The two sets of values are comparable except at θ_a = 150°, where S_{or} = 0.15 for the centrifuge and S_{or} = 0 for the waterflood. The discrepancy is likely due to a combination of factors. First, S_{oi} was smaller (= 0.77, 0.81) in the waterfloods than in the centrifuge experiments, which one would expect would give rise to smaller S_{or}. Second, while very small S_{or} have been predicted in pore network models [20] and may be explained by the establishment of oil layers on oil-wet grain surfaces through which oil can drains to low saturations [21, 22], it is unlikely that oil can remain connected until it drains to S_{or} = 0. Third, a premature change of rotation speed during the multi-speed centrifuge experiments at large ω may have resulted in an overestimation of S_{or} for the centrifuge experiment. Finally, it is also possible that centrifuge and waterflood establish different S_{or}. Further insight requires additional experiments on (cm-scale) cores and pore-scale visualization using, e.g., X-ray micro-computed tomography.

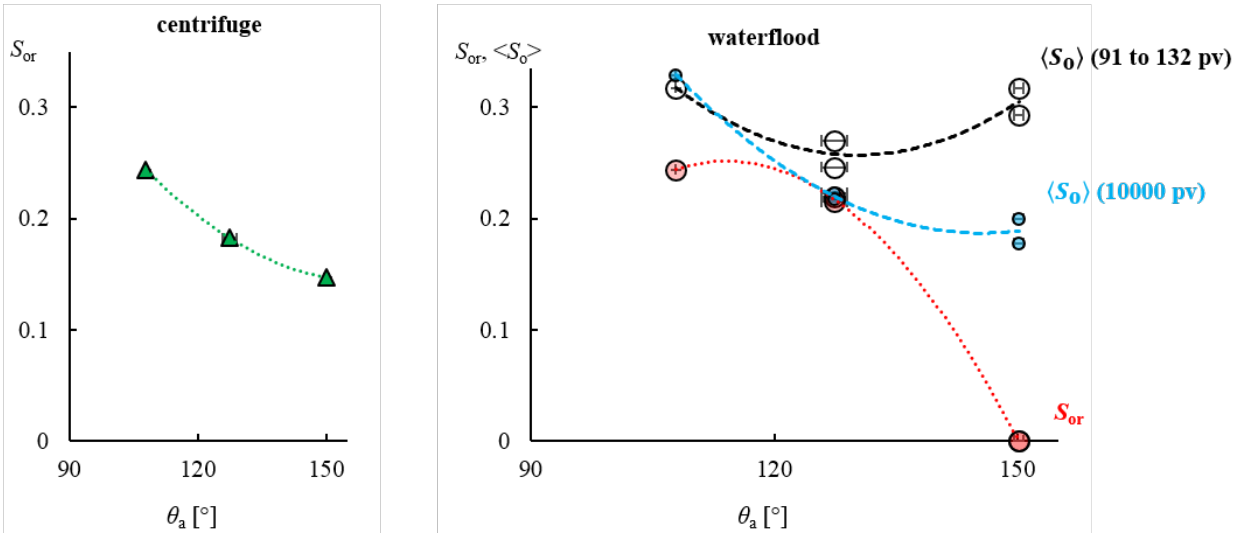

Figure 5. Residual oil saturation as measured by centrifuge (▲), core-averaged oil saturations after 91 to 132 pv (○, measured) [1 - 3] and 100000 pv (●, simulated) of water injection, and best-fit S_{or} to waterflood data (●). Horizontal bars are standard errors of the mean of contact angle measurements. Dotted and dashed lines are best-fit quadratic functions to the data, and are intended as guides to the eye.

The negative correlation between S_{or} and θ_a is in sharp contrast to the non-monotonic dependence of core-averaged oil saturation, $\langle S_o \rangle$, after 91 to 132 pv of water injection in the same rock/oil/water system (○) and by other authors in other systems [4, 5]. The disagreement arises from two factors: premature termination of the waterflood and capillary end effects. Simulations indicate that the equilibrium (steady state) had not been reached after ~100 pv at θ_a = 125° and 150°: indeed, after 10000 pv of water injection, $\langle S_o \rangle$ is monotonic (cyan ●). The difference between $\langle S_o \rangle$ (10000 pv) and best-fit S_{or} represents capillary end effects.

CONCLUSIONS

We present forced imbibition $P_c(S_w)$ curves and waterflood $k_r(S_w)$ curves for Indiana limestone under different mixed wettability conditions. The main findings are:

- S_{or} decreases with increasing contact angle from $\theta_a = 110°$ to 150° in both waterflood and centrifuge experiments.
- Thousands of pore volumes of water is necessary for a waterflood to reach equilibrium, i.e., for oil production to cease, at the largest θ_a.
- At $\theta_a = 110°$ and 150°, capillary end effects elevated the core-averaged equilibrium oil saturation at the end of the simulated waterflood by 9 and 20% of the pore volume, respectively, than the (true) S_{or}. These values are in good agreement with those reported by Masalmeh [15].
- At constant Ca, $k_{ro}(S_{wi})$ decreases monotonically with increasing θ_a.
- With realistic $k_w(S_w)$, $k_o(S_w)$, and $P_c(S_w)$ curves, S_{or} that decreases monotonically with contact angle can still give rise to a non-monotonic core-averaged oil saturation after $O(100)$ pv of water injection, i.e., a typical duration of a laboratory coreflood.

Huang & Honarpour [23] noted that capillary end effects were most pronounced when oil displaces water in water-wet cores and gas displaces oil. The discrepancy between waterflood S_{or} and core-averaged end-point saturation indicates that capillary end effects can also be significant when water displaces oil in mixed-wet rock, and highlights the importance of using simulation to interpret coreflood data under capillary-dominated conditions.

ACKNOWLEDGEMENTS

MC was supported by the University of Aberdeen College of Physical Sciences studentship, a Society of Petrophysicists and Well Log Analysts (SPWLA) Foundation grant, and an Aberdeen Formation Evaluation Society scholarship. The authors thank Blessing Akamairo for her assistance with one of the Indiana limestone/6.6×10^{-2} M cyclohexanepropionic acid/brine corefloods presented in Fig. 2. The authors thank Guillaume Lenormand at CYDAREX for helpful suggestions on their software CYDAR™ and reviewer Steffen Berg for his comments and suggestions.

REFERENCES

1. Christensen, M., Romanello, L. & Y. Tanino (2017) Greater-than-one relative permeability in mixed-wet limestone, *Proc.* International Symposium of the Society of Core Analysts, 27 Aug. - 1 Sept., SCA2017-103, Vienna, Austria.
2. Christensen, M. & Y. Tanino (2017) Waterflood oil recovery from mixed-wet limestone: dependence on contact angle, *Energy Fuel* 31(2): 1529–1535.
3. Christensen, M. & Y. Tanino (2017) Enhanced permeability due to apparent oil/brine slippage in limestone and its dependence on wettability, *Geophys. Res. Lett*. 44(12): 6116-6123.
4. Kennedy, H. T., Burja, E. O. & R. S. Boykin (1955) An investigation of the effects of wettability on oil recovery by water flooding, *J. Phys. Chem.* 59(9): 867-869.
5. Morrow, N. R., Cram, P. J. & F. McCaffery (1973) Displacement studies in dolomite with wettability control by octanoic acid, *Soc. Petrol. Eng. J.* 13(4): 221–232.

6. Jadhunandan, P. P. & Morrow, N. R. (1995). Effect of wettability on waterflood recovery for crude-oil/brine/rock systems, *SPE Reservoir Eng.*, SPE 22597: 40–46.
7. Amott, E. (1959). Observations relating to the wettability of porous rock. Trans. AIME, 216: 156–162.
8. Owens, W. W. & D. L. Archer (1971) The effect of rock wettability on oil-water relative permeability relationships, *J. Petrol. Technol*. 23(7): 873–878.
9. Lorentz, P. B., Donaldson, E. C. & Thomas, R. D. (1974). Use of centrifugal measurements of wettability to predict oil recovery. Technical Report 7873, USBM, Bartlesville Energy Technology Center.
10. Anderson, W. G. (1987). Wettability literature survey - part 4: effects of wettability on capillary pressure, *J. Petrol. Technol.* 39: 1283–1300.
11. Chen, J., Hirasaki, G. J. & Flaum, M. (2006). NMR wettability indices: effect of OBM on wettability and NMR responses, *J. Petrol. Sci.* 52: 161–171.
12. Romanello, L. (2015) Impact of wettability on relative permeability, MSc thesis, University of Aberdeen.
13. Tanino, Y. & M. J. Blunt (2012) Capillary trapping in sandstones and carbonates: dependence on pore structure, *Water Resour. Res.* 48(8), W08525: 1-13.
14. Tanino, Y. & M. J. Blunt (2013) Laboratory investigation of capillary trapping under mixed-wet conditions, *Water Resour. Res.* 49(7): 4311–4319.
15. Masalmeh, S. K. (2012) Impact of capillary forces on residual oil saturation and flooding experiments for mixed to oil-wet carbonate reservoirs, *Proc*., International Symposium of the Society of Core Analysts, 27 - 30 Aug., SCA 2012-11, Aberdeen, UK.
16. Forbes, P. (1994). Simple and accurate methods for converting centrifuge data into drainage and imbibition capillary pressure curves, *Log Analyst* 35(4): 31-53.
17. Lomeland, F., Ebeltoft, E. & W. H. Thomas (2005) A new versatile relative permeability correlation, *Proc.,* International Symposium of the Society of Core Analysts, 21-25 Aug., SCA2005-32, Toronto, Canada.
18. Tanino, Y., Akamairo, B., Christensen, M. & S. A. Bowden (2015) Impact of displacement rate on waterflood oil recovery under mixed-wet conditions, *Proc*., International Symposium of the Society of Core Analysts, 16-21 Aug., SCA2015-011, St. John's Newfoundland and Labrador, Canada.
19. Humphry, K. J., Suijkerbuijk, B. M. J. M., van der Linde, H. A., Pieterse, S. G. J. & S. K. Masalmeh (2013) Impact of wettability on residual oil saturation and capillary desaturation curves, *Proc*., International Symposium of the Society of Core Analysts, 16-19 Sept., SCA2013-025, Napa Valley, California.
20. Ryazanov, A. V., Van Dijke, M. I. J. & K. S. Sorbie (2009) Two-phase pore-network modelling: existence of oil layers during water invasion. *Transport Porous Med.* 80(1): 79-99.
21. Salathiel, R. A. (1973) Oil recovery by surface film drainage in mixed-wettability rocks, *J. Petrol. Technol.* 25(10): 1216 - 1224.
22. Blunt, M. J. (1998) Physically-based network modeling of multiphase flow in intermediate-wet porous media, *J. Petrol. Sci. Eng.* 20(3-4): 117-125.
23. Huang, D. D. & M. M. Honarpour (1998) Capillary end effects in coreflood calculations. *J. Petrol. Sci. Eng.* 19(1-2): 103-117.